Cent. Eur. J. Phys. • 6(3) • 2008 • 730-736
DOI: 10.2478/s11534-008-0046-9

VERSITA

Central European Journal of **Physics**

First-principles studies of the electronic structure and optical properties of $AgBO_3$ (B=Nb,Ta) in the paraelectric phase

Research Article

Suleyman Cabuk*, Sevket Simsek[1†]

Cukurova University, Faculty of Science and Letters, Physics Department, Adana, 01330, Turkey

Received 13 November 2007; accepted 29 January 2008

Abstract: The electronic energy-band structure, density of states (DOS), and optical properties of $AgBO_3$ in the paraelectric cubic phase have been studied by using density functional theory within the local density approximation for exchange-correlation for the first time. The band structure shows a band gap of 1.533 eV ($AgNbO_3$) and 1.537 eV ($AgTaO_3$) at (M-Γ) point in the Brillouin zone. The optical spectra of $AgBO_3$in the photon energy range up to 30 eV are investigated under the scissor approximation. The real and imaginary parts of the dielectric function and — thus the optical constants such as reflectivity, absorption coefficient, electron energy-loss function, refractive index, and extinction coefficient — are calculated. We have also made some comparisons with related experimental and theoretical data that is available.

PACS (2008): 71.15. Mb; 78.20.Ci; 77.84.Dy

Keywords: electronic structure • optical properties • $AgNbO_3$ $AgTaO_3$

1. Introduction

The Ag compounds $AgNbO_3$and $AgTaO_3$ belong to the ferroelectric perovskite family ABO_3. Silver niobate, $AgNbO_3$, has been reported by Francombe and Lewis to exhibit an orthorhombic distortion from the perovskite lattice at room temperature [1]. One of the first investigations of silver tantalate $AgTaO_3$ was performed by Francombe and Lewis, who determined an orthorhombic structure with a monoclinic distortion of the pseudo-cubic perovskite unit cell at room temperature [1]. $AgTaO_3$ is one of the less commonly investigated compounds among the ABO_3 perovskites. $AgBO_3$ is a ferroelectric and antiferroelectric perovskite system that has recently attracted attention due to its interesting microwave dielectric properties [2]. Because of recent developments in telecommunications, electro-optics, and piezoelectric components, perovskite niobates and tantalates have been placed on a short list of functional materials for future technologies [3].

$AgNbO_3$ and $AgTaO_3$ have a paraelectric phase with cubic symmetry when the temperature is above 903 K [4] and 758 K [5], respectively. As the temperature decreases, a series of structural phase transitions is observed in $AgNbO_3$ [6–10]. From literature data, $AgNbO_3$ undergoes the fol-

*E-mail: scabuk@cu.edu.tr
†E-mail: ssimsek_001@hotmail.com

lowing sequence of phase transitions :

$$M_1 \overset{340K}{\longleftrightarrow} M_2 \overset{540K}{\longleftrightarrow} M_3 \overset{626K}{\longleftrightarrow} O_1 \overset{634K}{\longleftrightarrow} O_2 \overset{660K}{\longleftrightarrow} T \overset{852K}{\longleftrightarrow} C$$

where M_1, M_2, and M_3 denote monoclinic distortions with orthorhombic symmetry, while O_1 and O_2 are the phases with orthorhombic symmetry. T and C denote the phases with tetragonal and cubic symmetry, respectively. The phase transition sequence of $AgTaO_3$ has been shown as follows [6] :

$$R \overset{663K}{\longleftrightarrow} M \overset{692K}{\longleftrightarrow} T \overset{777K}{\longleftrightarrow} C$$

where R indicates rhombohedral symmetry. In both $AgNbO_3$ (below 340 K) and $AgTaO_3$ (below 180 K), a weak indication of ferroelectricity has been detected [11, 12]. The electronic structure of niobiates and tantalates attract attention due to their interesting ferroelectric and relaxor properties. However, most of the papers devoted to $AgBO_3$ are focused on their structural and dielectric properties [13–16]. There are only a few studies of electronic structure of these compounds [17–19, 38–42]. The electronic structure of valence bands, the band gap, and the low-energy conduction band determine the most important properties of the material in electronic device application. In this work we have calculated, from first principles, the pseudopotential of the electronic band structure and optical properties of $AgBO_3$ in the cubic phase.

2. Calculation method

The crystal structure of $AgBO_3$ in the paraelectric phase has been studied experimentally using various techniques. The paraelectric phases are cubic and belong to the space group Pm3m (No. 221). There are five atoms of three types, the cubic unit cell. Ag is in the 1a position (0,0,0), B is located at the central position (1/2, 1/2, 1/2), and O takes the 3c position: (1/2, 1/2, 0), (1/2, 0, 1/2) and (0, 1/2, 1/2). The calculations were carried out using experimental data for lattice constant a = 3.9598 Å for $AgNbO_3$ [4] and a = 3.948 Å for $AgTaO_3$ [5]. The calculations presented in this paper stayed within the local density approximation (LDA) [20] of the density functional theory (DFT), as implemented in the FH198PP package [21], using the pseudopotential method. The self-consistent norm-conserving pseudopotentials are generated using the Troullier-Martins scheme [22]. Plane waves are used as a basis set for the electronic wave functions. In order to solve the Kohm-Sham equations [23], the conjugate gradient minimization method [24] is employed, as implemented by ABINIT code[1] [25]. The exchange correlation effects are taken into account within the Perdew-Wang scheme [26] as parameterized by Ceperley and Alder [27].

Pseudopotentials are generated using the following electronic configurations: For Ag[Kr], the $4d^{10}5s^1$electron is considered as the true valence. For Nb[Kr], $4d^45s^1$, and for Ta[Xe], $6s^25d^3$,electron states are treated as valence states. For O, only the true valence states ($2s^2$ and $2p^4$) are taken into account, because these states are enough to have the correct transferability property. The above configuration is found to be the optimized choice for these materials. All of the calculations involve a five atoms cubic unit cell arranged in a perovskite structure. We get a good convergence for the total-energy calculation with a cutoff energy of 32 a.u. for $AgNbO_3$ and 33 a.u. for $AgTaO_3$, using a $8 \times 8 \times 8$, Monkhorst-Pack [28] mesh grid. We have found that in the band structure calculations 67k points are enough to obtain good results for these transition-metal oxides. In the density of states calculations, however, the irreducible Brillouin zone was sampled with 512k points for $AgBO_3$.

3. Results and discussions

3.1. Structure parameters

The calculations first were carried out using the experimental data for lattice constants. Then, by minimizing the ratio of the total energy of the crystal to its volume, the theoretical lattice constants were obtained for cubic $AgBO_3$, as shown in Table 1. We compare the present results for lattice parameters of $AgBO_3$ with previous theoretical and experimental values. This is within the accuracy range of calculations based on density functional LDA.

[1] *http:// www.abinit.org/*

Table 1. Comparison of present results for lattice parameters of cubic $AgBO_3$ with previous theoretical and experimental values.

	Ref.	Lattice parameter [Å]	Error [%]
$AgNbO_3$:			
(LDA) PW-CA	(this work)	a = 3.9584	0.035
VASP	[29]	a = 7.9088	99.7
Experimental value	[4]	a = 3.9598	-
$AgTaO_3$:			
(LDA) PW-CA	(this work)	a = 3.9545	0.16
Experimental value	[5]	a = 3.9480	-

3.2. Band structure

The calculated electronic band structure for paraelectric $AgBO_3$ in high-symmetry directions in the Brillouin zone is shown in Fig. 1 and 2. The Fermi level (E_F) is set as zero of energy and indicated by a horizontal dashed line. High-symmetry points in the Brillouin zone include Γ (0,0,0), X (0,1/2,0), M (1/2,1/2,0), and R (1/2,1/2,1/2). The general features of the energy bands are similar for both oxides. In both crystals, the bottom band between about -18 eV and -16 eV originate from the O 2s orbital. The valence band exists from -18 eV to 0 for both compounds. The top of the valence band for cubic $AgBO_3$ consists of mainly O 2p. Also O 2p is hybridized with Ag 4d and somewhat with B nd orbitals (n=4 and 5 for Nb and Ta, respectively). However, the conduction band consists of mainly B nd from 1.64 eV to 12 eV (for $AgNbO_3$) and 1.82 eV to 11.50 eV (for $AgTaO_3$). So, electron excitation happens from O 2p and (O 2p+Ag 4d) to B nd. The excited electrons on B are responsible for reduction, and the holes left on O are responsible for oxidation. The contribution of Ag atoms to the bands of B nd is very small because of the large distance between Ag and B atoms. Ag 5s and 5p, which are unoccupied and somewhat localized, contribute a little to the conduction band. An unoccupied Ag 5s and 5p orbital covers the conduction band at an energy level from 12 eV to 22.67 eV (for $AgNbO_3$) and 11.50 eV to 22.5 eV (for $AgTaO_3$). Ag 5s and Ag 5p cover the latter part of the conduction band from 12 eV to 22.67 eV (for $AgNbO_3$) and 11.50 eV to 22.5 eV (for $AgTaO_3$), which somewhat overlap but are not hybridized with B nd, as judged from the different band shape. It is found to be in agreement with the valence bands of $AgNbO_3$ single crystals and ceramics determined by x-ray photoemission spectroscopy (XPS) measurements of a valence band width of about 6.5 eV [19]. The valence bands are separated from the conduction bands at the symmetry point (Γ) by a direct gap of 2.933 eV for $AgNbO_3$ and 2.908 eV for $AgTaO_3$. In both $AgNbO_3$ and $AgTaO_3$, an indirect band gap appears between the top-most valence band at the M point and the bottom-most conduction bands at the Γ point. Our calculated values of the indirect band gaps of Ag(Nb,Ta)O_3 are 1.533 eV and 1.537 eV, respectively. These calculated values are smaller than experimental values estimated from the onset of absorption, which is 2.8 eV for $AgNbO_3$ and 3.4 eV for $AgTaO_3$ [18]. It is well known that the band gap calculated by DFT is smaller than that obtained from experiments. This error is due to the discontinuity of exchange-correlation energy. Therefore a scissors operator was needed to shift all the conduction levels to agree with the measured value of the band gap, which we applied to the calculation of optical parameters.

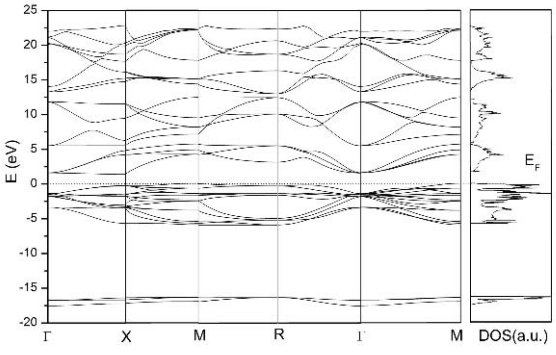

Figure 1. Band structure along the high symmetry directions in the Brillouin zone and DOS of $AgNbO_3$.

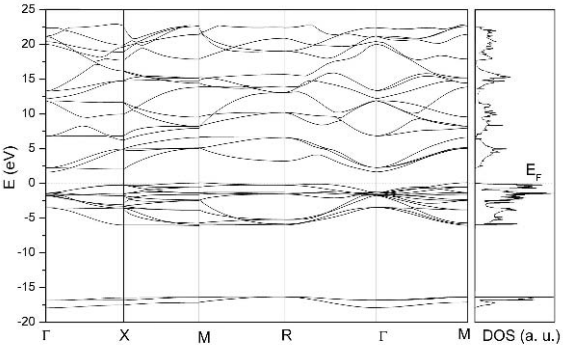

Figure 2. Band structure along the high symmetry directions in the Brillouin zone and DOS of $AgTaO_3$.

The band gaps are computed very accurately, using the so-called GW approximation [30]. The origin of this discrepancy may be the LDA , which underestimates the band gaps even for insulators. To further elucidate the nature of electronic band structure, the DOS have been calculated by the tetrahedral method [31] for both crystals shown in the right panels of Fig. 1 and 2. The DOS for $AgBO_3$in both calculations are quite similar to each other. The electronic structure and DOS for $AgTaO_3$ are in agreement with the ones calculated by the CASTEP program [18].

3.3. Optical properties

The optical response of crystals can be described by the complex dielectric function $\varepsilon(q,\omega)$, where q is the momentum transfer in the electron-photon interaction and ω is the energy transfer. The (q=0) dielectric function was calculated in the momentum representation, which requires matrix elements of momentum $\vec{P}$ between occupied and unoccupied eigenstates. To be specific, the imaginary part of the dielectric function, $\varepsilon_2(\omega) = Im\varepsilon(q=0,\omega)$ was calculated from [32]

$$\varepsilon_2^{ij}(\omega) = \frac{4\pi e^2}{\Omega m^2 \omega} \sum_{Knn'} \left\langle \vec{K}n\sigma \left| P_i \right| \vec{K}n'\sigma \right\rangle \left\langle Kn'\sigma \left| P_j \right| Kn\sigma \right\rangle \cdot f_{Kn}(1-f_{Kn'})\delta(E_{Kn'} - E_{Kn} - \hbar\omega) \quad (1)$$

In Eq. (1), e is the electron charge, m is its mass, Ω is the volume, and f_{Kn} is the Fermi distribution. Moreover, $\left|\vec{K}n\sigma\right\rangle$ is the crystal wave function corresponding to the n-th eigenvalues, with crystal momentum $\vec{K}$ and spin σ. The summation over the Brillouin zone Eq. (1) is calculated using a linear interpolation on a mesh of uniformly distributed points. Matrix elements, eigenvalues, and eigenvectors are calculated in the irreducible part of the Brillouin zone. The correct symmetry for the dielectric constant was obtained by averaging the calculated dielectric function. A major problem with LDA calculations of dielectric constant $\varepsilon = 1 + 4\pi\chi$ is the underestimation of the band gap. Because the Kohn-Sham equation determines ground-state properties, the unoccupied conduction bands that appear in the calculations have no physical significance. If they are used as single-particle states in a calculation of optical properties for semiconductors or insulators, a band problem comes into existence: The absorption begins at too low an energy. In LDA calculations, it is common practice to apply a scissors operator approximation [30, 33, 34] to compensate for the lack of polarization dependence of the exchange-correlation functional. The discussion above concerning the band-gap problem suggests that one should choose scissors shift $\Delta = E_{gap}^{exp.} - E_{gap}^{LDA}$ [30]. We therefore estimate the correction to the band gap on the basis of the difference between the calculated LDA band gap and the experimental optical gap [18]. In the present work, Δ is 1.27 eV ($AgNbO_3$) and 1.86 eV ($AgTaO_3$). Finally the real part of the dielectric function $\varepsilon_1(\omega)$ is obtained from $\varepsilon_2(\omega)$ using the Kramers-Kroning transformation,

$$\varepsilon_1 = Re[\varepsilon(q=0,\omega)] = 1 + \frac{1}{\pi}\int_0^\infty \varepsilon_2(\omega')\left(\frac{1}{\omega'-\omega} + \frac{1}{\omega'+\omega}\right)d\omega' \quad (2)$$

Using the method mentioned above, we calculated the imaginary (ε_2) and real (ε_1) parts of $\varepsilon(\omega) = \varepsilon_1(\omega) - i\varepsilon_2(\omega)$ between 0 and 30 eV for $AgBO_3$, and the results are shown Fig. 3(a) and (b). Solid line indicates the function for $AgNbO_3$ and dotted line for $AgTaO_3$. In order to account for the structures observed in the optical spectra, it is customary to consider transitions from occupied to unoccupied bands in the electronic energy band structure, especially at high symmetry points in the Brillouin zone. For the absorptive part of the dielectric function ε_2, for$AgNbO_3$, shown in Fig. 3(a), the highest peak in ε_2 at $\sim$ 8.8 eV arises from O 2p → Nb 4d t_{2g} at the M point. For $AgTaO_3$, the value of the main peak of the ε_2 curve in Fig. 3(a) is 11.19 eV, which arises from O 2p → Ta 5d t_{2g} at the M point. These are followed by other, smaller peaks between 10 and 20 eV for $AgNbO_3$and 12-20 eV for $AgTaO_3$. The minimum in ε_2 occurs at about 13 eV ($AgNbO_3$ and $AgTaO_3$). The real parts of the dielectric function are shown in Fig. 3(b) for $AgBO_3$ in the cubic phase. The first peak in ε_1 at about 4.62 eV ($AgNbO_3$) and 4.97 eV ($AgTaO_3$) originates from O 2p → Nb 4d and O 2p → Ta 5d at probably the Γ point or the X point, respectively. This peak is followed by a decrease, which reaches a global minimum at 12.40 eV ($AgNbO_3$) and 12.28 eV($AgTaO_3$), and fairly small peaks between 12.5 and 20 eV for $AgBO_3$. The $\varepsilon_1(0)$ values of $AgBO_3$ in the cubic phase are 2.843 ($AgNbO_3$) and 3.013 ($AgTaO_3$).

The optical properties may be extracted from knowledge of the complex dielectric function. Expressions for optical constants like refractive index $n(\omega)$, extinction coefficient $k(\omega)$, absorption coefficient $\alpha(\omega)$, reflectivity $R(\omega)$, and energy loss spectrum $L(\omega)$ now follow immediately as given below [35]:

$$n(\omega) = (1/\sqrt{2})[\varepsilon_1(\omega) + \sqrt{\varepsilon_1^2(\omega) + \varepsilon_2^2(\omega)}]^{1/2}$$

$$k(\omega) = (1/\sqrt{2})[\sqrt{\varepsilon_1^2(\omega) + \varepsilon_2^2(\omega)} - \varepsilon_1(\omega)]^{1/2}$$

$$\alpha(\omega) = \sqrt{2}\omega[\sqrt{\varepsilon_1^2(\omega) + \varepsilon_2^2(\omega)} - \varepsilon_1(\omega)]^{1/2} \quad (3)$$

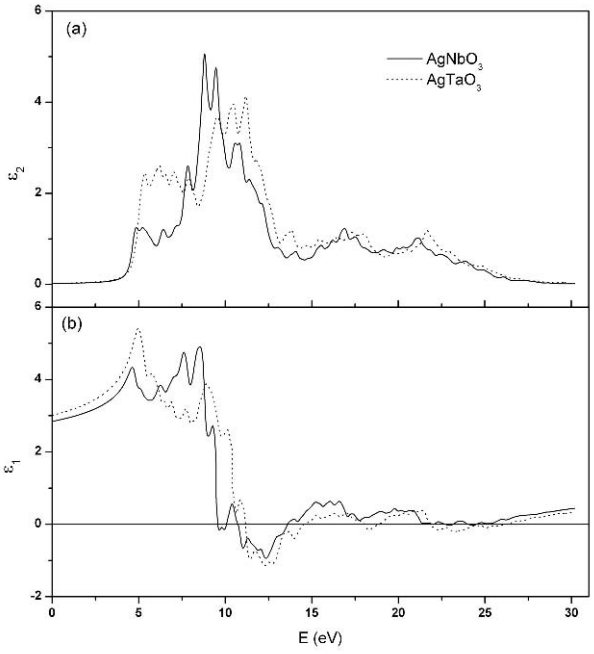

Figure 3. The imaginary parts (a) and the real parts (b) of complex dielectric function for $AgBO_3$.

$$R(\omega) = \left| \frac{\sqrt{\varepsilon(\omega)} - 1}{\sqrt{\varepsilon(\omega)} + 1} \right|^2$$

$$L(\omega) = \frac{\varepsilon_2(\omega)}{\varepsilon_1^2(\omega) + \varepsilon_2^2(\omega)}$$

We have derived $n(\omega)$, $k(\omega)$, $\alpha(\omega)$, $R(\omega)$, and $L(\omega)$ of $AgBO_3$ in the energy range up to 30 eV using Eq. (3). The reflectivity spectra for $AgBO_3$ are shown as a function of energy in Fig. 4(a). This could possibly make the compound $AgBO_3$ suitable for a variety of optical application. The static refractive index values for $AgBO_3$ in the cubic phase calculated in this work are shown in Fig. 4(b). We obtain n(0) as 1.686 ($AgNbO_3$) and 1.736 ($AgTaO_3$) for the cubic phase. The maximum $n(\omega)$ of 2.092 ($AgNbO_3$) and 2.348 ($AgTaO_3$) were found. The refractive index for $AgBO_3$ increases with energy in the transparency region, reaching a peak in the ultraviolet at about 5 eV, due probably to interband transitions. Then they decrease to a minimum level of about 12.5 eV. The calculated extinction coefficients for $AgBO_3$ are presented in Fig. 4(c). As can be seen from Fig. 4(c), normal dispersion exists in the 0–3.5 eV energy range. This is consistent with results for ε_2 in Fig. 3(a). The calculated linear absorption spectrum is displayed in Fig. 4(d) for $AgBO_3$. $\alpha(\omega)$ is very large (about 10^4 cm^{-1}) and decreases rapidly in the low-energy region. The fundamental absorption edge starts from about 3.3 eV for $AgNbO_3$ and 3.2 eV for $AgNbO_3$, which correspond to the direct Γ–Γ transition. This originates from the transition from the O 2p electron states located at the top of the valence to the empty Nd 4d ($AgNbO_3$) and Ta 5d ($AgTaO_3$) electron states dominating the bottom of the conduction bands. The loss function $L(\omega)$ describes the energy loss of a fast electron traversing the material. The electron energy-loss functions $L(\omega)$ of $AgBO_3$ were calculated from Eqs. (3). This is displayed in Fig. 4(e). In the energy region above 15 eV there is a drop in ε_2, and there is no sharp structure in its spectrum, which corresponds to exhaustion of the sum rule and the excitation of plasma vibrations in the valence band. At energies in excess of 15 eV, the spectrum of $L(\omega)$ includes a wide band associated with the excitation of the 2p valence electrons of oxygen. The present spectra of $L(\omega)$ exhibit maxima both at the energy of the interband transitions and at the energies of the plasma resonances (Fig. 4(e)). Analysis of $L(\omega)$ determines the energy of the plasma oscillation of the valence electrons E_p= 25.567 eV ($AgNbO_3$) and 26.498 eV ($AgTaO_3$). In addition the peaks of $L(\omega)$ also correspond to the trailing edge in the reflection spectra, for instance, the peak of $L(\omega)$ at 13.575, 25.567 eV ($AgNbO_3$) and 14,367, 26.498 eV ($AgTaO_3$) corresponding to the abrupt reduction of $R(\omega)$. The other peaks arise at the valence bands to the lower and upper conductions bands.

Unfortunately, we are not able to find any experimental results and theoretical calculations for optical properties of cubic $AgBO_3$ in the energy region close to the fundamental absorption edge, except [18]. We expect that our theoretical studies will motivate experimental work aimed at investigating the optical properties of the cubic phase of this compound.

3.4. Sum rule and effective number of valence electrons

From the known sum rules [36] we can determine certain quantitative values, particularly the effective number N_{eff} of the valence electrons and the effective optical dielectric constant ε_{eff}, which contribute to the optical constant of the crystal at the frequency ω_0. Recall that

$$N_{eff} = \frac{m}{2\pi e^2} \frac{1}{N_a} \int_0^{\omega_0} \omega \varepsilon_2(\omega) d\omega \qquad (4)$$

$$\varepsilon_{eff} = 1 + \frac{2}{\pi} \int_0^{\omega_0} \omega^{-1} \varepsilon_2(\omega) d\omega \qquad (5)$$

where N_a is the density of the atoms in the crystal. The quantities m and e are the electron mass and charge re-

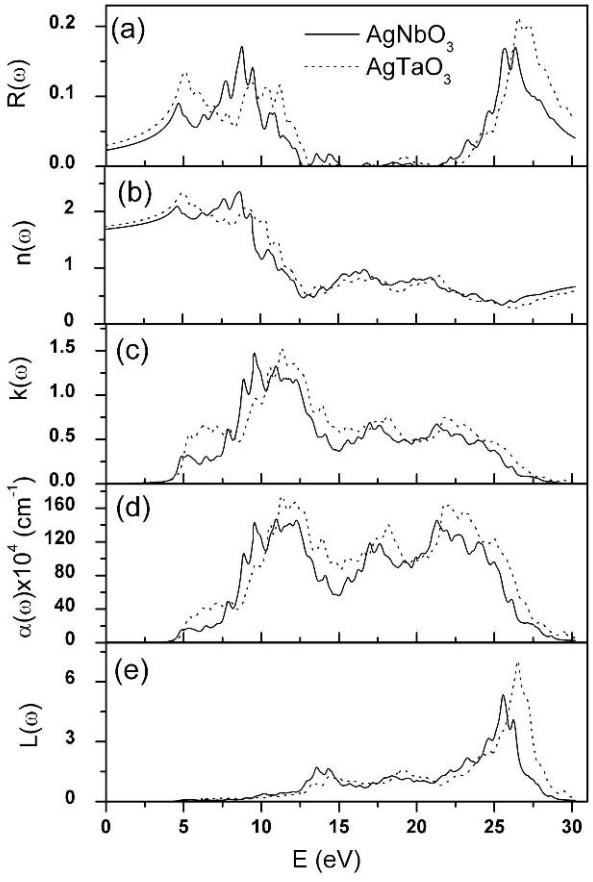

Figure 4. The calculated (a) reflectivity spectra, (b) refractive index, (c) extinction coefficient, (d) absorption coefficient, and (e) electron energy–loss spectrum for $AgBO_3$.

spectively. The physical meaning of ε_{eff} is quite clear: ε_{eff} is the effective optical dielectric function governed by interband transition in the internal frequency from zero to ω_0 , that is, by the polarization of the electron shell. Each of our plots of ε_{eff} vs. photon energy for $AgBO_3$ (Fig. 5(a)) can be arbitrarily divided into two parts. The first part is characterized by a rapid growth of ε_{eff} and extends up to 12 eV. The second part shows a smoother and slower growth of ε_{eff} and tends to saturate at energies above 25 eV. This means that the largest contribution to ε_{eff} is made by transitions corresponding to the bands at $\sim$ 5 eV and $\sim$12 eV. (Their contribution amounts to $>$ 80%.) To determine the contribution made to the static dielectric function $\varepsilon(0)$ by transition with frequency $\omega > \omega_0$,we compare the maximum ε_{eff} with the square of the refractive index ($n^2 = \varepsilon(0)$) measured in the transparency region [37]. The difference $\delta\varepsilon = \varepsilon(0) - \varepsilon_{eff} > 0$ points to the need for taking into account the polarizability of the deep levels. The obtained difference $\delta\varepsilon = \varepsilon(0) - \varepsilon_{eff}$ ($\delta\varepsilon$ =0.1 for $AgNbO_3$ and 0.07 for $AgTaO_3$) indicates a large contribution of transitions with $\omega > \omega_0$ to the static dielectric constant. This means that the greatest contribution to ε_{eff} arises from the interband transition between 5 eV and 25 eV.

On the other hand, the N_{eff} determined from the sum rule is the effective number of valence electrons per crystal atom at the energy $\}\omega$ (under the condition that all the interband transitions possible at this frequency $\omega_0$were made). The photon energy dependence of the $N_{eff}$is shown in Fig. 5(b). The effective valence electron number up to 4.8 eV is zero (below the band gap), then rises rapidly at low energy and saturates at about 28 eV , with a value of 27.8 ($AgTaO_3$) and 24.5 eV ($AgNbO_3$) for the effective electron number. These show that the deep-lying valence orbital participates in the interband transition.

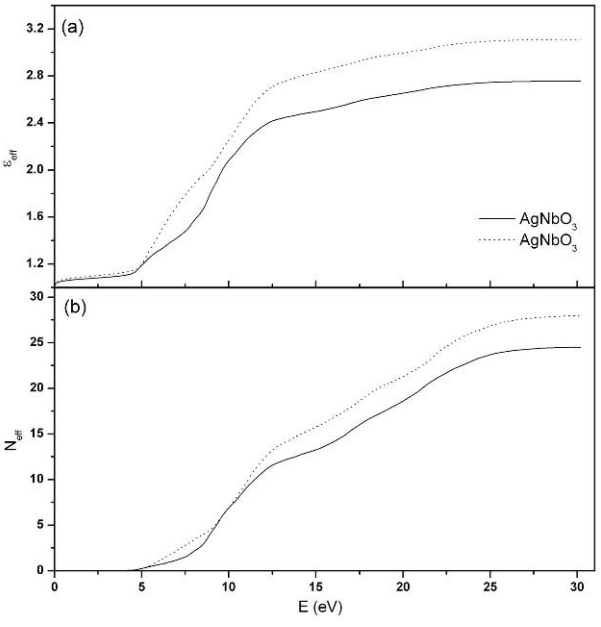

Figure 5. The calculated (a) effective optical dielectric constant and (b) effective number of electrons participating in the interband transitions.

4. Conclusions

We calculated the electronic structure, the total DOS, and optical properties of $AgBO_3$ in the paraelectric cubic phase using ABINIT code in a wide energy range. The results yield lattice constants that are in agreement with experimental studies. The calculation shows that the band gap is indirect (M-Γ). Our calculated fundamental gap is 1.533 eV ($AgNbO_3$) and 1.537 eV ($AgTaO_3$),

which is less than the experimental value, due to LDA underestimation. The optical properties, such as the dielectric function, reflectivity, absorption coefficient, electron energy-loss function, refractive index, extinction coefficient, ε_{eff}, and N_{eff} have been analyzed for the interband contribution to the optical response functions. It is found that the origin of peaks in the dielectric function probably also explains the structures in the spectra of these optical functions. We are not aware of any published data of electronic structure and optical properties of cubic $AgBO_3$, so our calculations can be used to cover this lack of data for these crystals.

Acknowledgments

The authors are grateful to ABINIT group for their ABINIT project that we used in our computations. This work was supported by Cukurova University under FEF2006YL80 project number.

References

[1] F. Jona, G. Shirane, Ferroelectric Crystals (Dover Publications Inc., New York, 1993)
[2] W. Fortin, G.E. Kugel, J. Griges, A. Kania, J. Appl. Phys. 79, 4273 (1996)
[3] F. Zimmermann, W. Menesklou, E.J. Ivers-Tiffee, J. Euro. Cer. Soc. 24, 1811 (2004)
[4] Ph. Sciau, A. Kania, D. Dkhil, E. Suard, A. Ratuszna, J. Phys.–Condens. Matter 16, 2795 (2004)
[5] G.E. Kugel et al., J. Phys. C 20, 1217 (1987)
[6] M. Pawelczyk, Phase Trans. 8, 273 (1987)
[7] M. Verwerft et al., Phys. Status Solidi A 112, 451 (1989)
[8] A. Kania, Ferroelectrics 205, 19 (1998)
[9] A. Ratuszna, J. Pawluk, A. Kania, Phase Trans. 7, 64. (2003)
[10] J. Sucharicz, A.Kania, G. Stopa, R. Bujakiewicz-Koronska, Phase Trans. 80, 123 (2007)
[11] A. Kania, K. Roleder, M. Lukaszewski, Ferroelectrics 52, 205 (1984)
[12] A. Kania, K. Roleder, Ferroelectric Lett. 2, 51 (1984)
[13] E. Buixaders, S. Kamba, J. Petzelt, Ferroelectrics 308, 131 (2004)
[14] A.A. Volkov et al., J. Phys.–Condens. Matter 7 , 785 (1995)
[15] M. Volant, D. Suvorov, C. Hoffmann, H. Sommoriva, J. Eur. Cer. Soc. 21, 2647 (2001)
[16] A. Kania, J. Kwapulinski, J. Phys.–Condens. Matter 11, 8933 (1999)
[17] A.A. Ivantsov et al., Phys. Status Solidi B 164, K23 (1991)
[18] H. Kato, H. Kobayashi, A. Kudo, J. Phys. Chem. B 106, 12441(2002)
[19] M. Kruczek, E. Talik, A. Kania, Solid State Commun. 137, 467 (2006)
[20] R. Cohen, H. Krakauer, Phys. Rev. B 42, 6416 (1990)
[21] M. Fuch, M. Scheffler, Comput. Phys. Commun. 119, 67 (1999)
[22] N. Troullier, J.L. Martins, Phys. Rev. B 43, 1993 (1990)
[23] W. Kohn, L.J. Sham, Phys. Rev. 140, A1133 (1965)
[24] M.C. Payne et al., Rev. Mod. Phys. 64, 1045 (1992)
[25] X. Gonze et al., Comp. Mater. Sci. 25, 478 (2002)
[26] J.P. Perdew, Y. Wang, Phys. Rev. B 45, 13244 1992
[27] D.M. Ceperley, B.J. Alder, Phys. Rev. Lett. 45, 566 (1980)
[28] H.J. Monkhorst, J.D. Pack, Phys. Rev. B 140, A1333 (1976)
[29] S.A. Prosandeev, Phys. Solid State 47, 2130 (2005)
[30] W.G. Aulbur, L. Jonsson, J.W. Wilkins, Solid State Phys. 54, 1 (2000)
[31] P.E. Blöchl, O. Jepsen, O.K. Andersen, Phys. Rev. B 49, 16222 (1994)
[32] M. Fox, Optical Properties of Solids (Oxford University Press, Oxford, UK, 2002)
[33] J.L.P. Hughes, J.E. Sipe, Phys. Rev. B 53, 10751 (1996)
[34] Z.H. Levine, D.C. Allan, Phys. Rev. Lett. 66, 41 (1991)
[35] R.E. Hummel, Electronic Properties of Material, 3rd edition (Springer + Business Media, Inc., New York, 2001)
[36] D. Pines, Elementary Exications in Solids (Benjamin Inc., New York – Amsterdam, 1963)
[37] E.I. Gerzanich, V.A. Lyakhovitskaya, V.A. Fridkin, B.A Popovkin, Current Topics in Materials Science SbSI and other Ferroelectric $A^{V}B^{IV}C^{VII}$Materials (North-Holland, Amsterdam, 1982)
[38] Z. H. Li, G. Chen, J. W. Lui, Solid State Commun. 143, 295 (2007)
[39] S. Cabuk, H. Akkus, A.M. Mamedov, Physica B 394, 81 (2007)
[40] S. Saha, T.P. Sinha, A. Mookerjee, Eur. Phys. J. B 18, 207 (2000)
[41] S. Saha, T.P. Sinha, Phys. Rev. B 62, 8828 (2000)
[42] M. Veithen, Ph. Ghosez, Phys. Rev. B 65, 214302 (2002)